Far-field spectral characterization of conical emission and filamentation in Kerr media

Daniele Faccio,* Paolo Di Trapani, Stefano Minardi,† and Alberto Bramati‡

Instituto Nazionale per la Fisica della Materia and Department of Physics and Mathematics, University of Insubria, Via Valleggio 11, I-22100 Como, Italy

Francesca Bragheri, Carlo Liberale, and Vittorio Degiorgio

Instituto Nazionale per la Fisica della Materia and Department of Electronics, University of Pavia, Via Ferrata 1, I-27100 Pavia, Italy

Audrius Dubietis and Aidas Matijosius

Department of Quantum Electronics, Vilnius University, Sauletekio Ave. 9, Building 3, LT-2040, Vilnius, Lithuania

Received May 12, 2004; revised manuscript received October 6, 2004; accepted October 23, 2004

By use of an imaging spectrometer we map the far-field (θ–λ) spectra of 200-fs optical pulses that have undergone beam collapse and filamentation in a Kerr medium. By studying the evolution of the spectra with increasing input power and by using a model based on an asymptotic linear superposition of stationary wave modes (rather than the exact instantaneous solution), we are able to trace a consistent model of optical beam collapse highlighting the interplay between conical emission, multiple pulse splitting, and other effects such as spatial chirp.

OCIS codes: 190.5940, 320.2250.

1. INTRODUCTION

Filamentation and, in general, collapse of high-power laser pulses in transparent media has attracted significant attention since its prediction[1,2] and observation[3,4] and, owing to the complexity of the involved phenomena, continues to be a hotly debated topic. There are many reasons for this interest, ranging from application possibilities such as the localization of ultrashort laser pulses over long propagation distances,[5] white-light laser sources for parametric amplification[6] or spectroscopy,[7,8] or the formal analogy with equations that describe nonlinear wave collapse in other systems, such as Bose–Einstein condensates,[9] that are experimentally less accessible. Numerical investigation of optical wave collapse is usually carried out starting from the nonlinear Schrödinger equation that describes the spatial evolution of a beam considering diffraction and a self-focusing term that originates from the real part of the third-order medium Kerr nonlinearity (n_2). Such an equation predicts the formation of an unstable two-dimensional stationary solution, the so-called Townes profile,[1] that, if perturbed, will either diffract or undergo catastrophic collapse. However, ultrashort laser pulses do not, in general, follow this behavior[10]: The collapse is arrested by other effects such as pulse lengthening due to normal group-velocity dispersion (GVD) or plasma defocusing and an apparently stationary propagation regime (filament) is reached. Thus the nonlinear Schrödinger equation may be accordingly modified to account for space–time coupling and also for plasma generation and defocusing. These modified equations have proved to be able to describe many of the phenomena associated with pulse filamentation such as conical emission (CE),[11] super-continuum generation, pulse steepening,[12] and splitting.[13] One of the main features that is emerging is the importance of space–time coupling. Indeed, there exist regimes characterized simultaneously by ultratight focusing and ultrashort pulse lengths in which the nonlinearity couples the spatial and temporal dynamics following an underlying geometry dictated by the modulational instability gain profile.[11,14] In such cases it is preferable to avoid space–time separation and refer directly to the geometrical properties of the space–time environment. A measure of the importance of these new concepts is given, for example, by the discovery of nonlinear X waves,[15–18] chaotic spatiotemporal fragmentation due to space-time modulational instability,[19] red solitons,[20] X waves in pulse filamentation,[21] and stationary conical waves supported by nonlinear losses.[22] The complexity of these issues requires a careful examination of the experimental methods employed, as space–time coupled phenomena should be investigated with adequate instruments.

We note that the major part of laser physics diagnostics is based on the separation of spatial and temporal effects leading, for example, to the widely used concepts of carrier spatial and temporal frequencies, beam walk-off and group velocity, diffraction and dispersion, etc., i.e., either purely spatial or purely temporal quantities. This conceptual space–time division is also reflected in the standard experimental characterization methods also adopted

for the study of beam filamentation. We have on the one hand near- and far-field imaging that give information on the spatial profiles but ignore the temporal profile. On the other hand, temporal autocorrelation traces or frequency resolved optical gating (FROG) give a precise measurement of the temporal profile at the medium output of the whole (or a particular portion of the) filament,[13,23,24] thus losing any information regarding the (transverse) space-dependent temporal profile. The limitations of FROG measurements have been partly overcome with the so-called SPIDER technique[25] that gives the temporal profile across one spatial dimension[26] and by use of a particular three-dimensional optical gating method[27,28] that provides the full spatiotemporal intensity profile of femtosecond pulses and has indeed allowed a full dimensional intensity space–time characterization of filaments in water[29] and of X waves in $\chi^{(2)}$ media.[28] Although extremely powerful, this technique requires the use of two separate, high-power, synchronized laser sources, the first providing the pulse under investigation and the second providing a pulse that must have an appreciably shorter time duration in order to guarantee a high (temporal) resolution. Moreover, this method is based on a second-order nonlinear upconversion process: Owing to the large (spatial and temporal) bandwidths involved, it is necessary to resort to very thin (20 μm or less) conversion crystals that in turn lead to low output powers and the necessity to integrate over many pulses.

Here we propose another possible experimental investigation tool, namely far-field spectral (θ–λ) characterization, that may give readily accessible details of the spatiotemporal pulse profile in single-shot acquisition. This method can be used as a general investigation tool for phenomena that involve space–time coupling, and we show its application to pulse filamentation in normally dispersive Kerr media. To the best of our knowledge there are only a few papers in literature that show the angular (θ–λ) spectra of Kerr-induced filaments[10,30,31] and none of which actually pay attention to the details these may contain, and certainly no systematic study in this sense has been carried out before. The data we present here are tentatively explained with the aid of a simple interpretation model based on a linear description of the stationary asymptotic light wave modes that act as attractors during the pulse evolution.[32]

2. SURVEY OF BEAM COLLAPSE AND FILAMENTATION OF FEMTOSECOND PULSES

In this paper we used a normally dispersive Kerr medium with a fixed total length, and the only variable parameter was the input pulse energy. Therefore we give here a brief overview of the expected pulse evolution for increasing input energies based on the existing literature.

For very low powers no self-focusing (SF) occurs, and the beam behaves linearly. However, with increasing power the threshold for catastrophic self-focusing is reached and the beam will start to spatially contract. A simple expression for the critical power for cw Gaussian beams is given by[33]

$$P_{\mathrm{crit}} = \frac{3.77\lambda^2}{8\pi n_0 n_2}, \tag{1}$$

where the nonlinear refractive index is given as a function of the pulse intensity I by $n = n_0 + n_2 I$. If the medium dispersion is also accounted for, then, the threshold for SF, in general, will be higher for short pulses than for longer ones owing to the damping effect of normal GVD, and Eq. (1) should be modified accordingly.[34,35] It has also been noted that the threshold for SF coincides with that for spectral broadening,[36] another manifestation of the material nonlinearity in the form of a rapidly time-varying self-phase modulation (SPM). For powers just above P_{crit} the beam will contract spatially, and the energy will move toward the back of the pulse and will eventually lead to pulse steepening and the formation of a shock wave at the trailing edge.[12,37,38] The intensities reached by the pulse give rise to efficient CE, whereas pulse steepening may explain the observed higher conversion efficiencies for the anti-Stokes (blueshifted) components.[12] As the power is further increased ($P \sim 1.5$–$2P_{\mathrm{crit}}$), the pulse will undergo temporal splitting[37,38] owing to the effect of normal GVD. Even higher powers ($P > 3P_{\mathrm{crit}}$) will lead to a pulse that evolves by pushing the energy toward the leading edge.[37,39–41] The peak intensities have been shown to be sufficient to excite a plasma with a large enough concentration as to even compensate the Kerr-induced refractive index variation.[36,42] The same plasma will eventually reduce the peak intensity through absorption, but multiple-pulse reformation for sufficiently high powers occurs, with each new pulse rising from the trailing background power.[39,40] Alongside an evident CE it has been observed that a large part of the generated spectrum is actually emitted along the pulse propagation axis.[43] This has been explained by considering a possible Kerr-lensing effect induced by the pulse itself[36] or possibly by the formation of an effective waveguide.[44] From this brief overview we can see that a large number of phenomena are involved, some occurring simultaneously, whereas the presence of others depends on the particular input conditions. In the following sections we describe the experimental investigation method and results that shed some new light on the details of the filamentation process.

3. EXPERIMENTAL SETUP

We present data concerning filamentation in a 15-mm-long type II lithium triborate (LBO) crystal. Such crystals are usually used for experiments involving the second-order [$\chi^{(2)}$] nonlinearity; however, we rotated the crystal so that all second-order processes are severely phase mismatched (and thus negligible) while still maintaining the pump-pulse propagation axis perpendicular to the input facet. The input laser pulse is delivered from a frequency-doubled 10-Hz Nd:glass mode-locked and regeneratively amplified system (TWINKLE, Light Conversion, Lithuania) and has a 200-fs duration and a 527-nm central wavelength. Spatial filtering of the pulse before the sample is entered is necessary for a guaranteed uniform Gaussian-like profile that will thus seed only one filament at a time (i.e., no spatial breakup into multiple

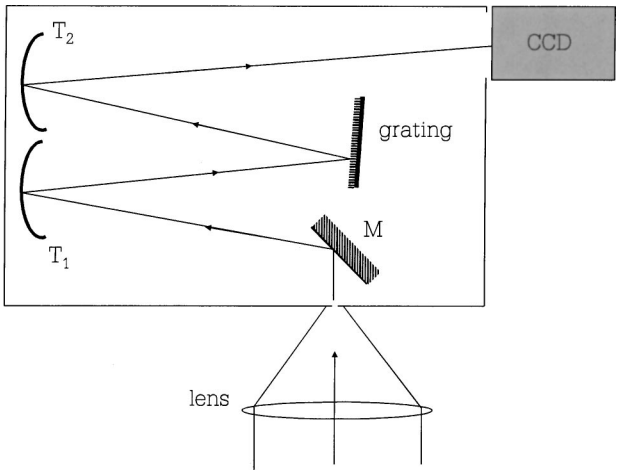

Fig. 1. Experimental layout of the imaging monocromator used for the measurements. T_1 and T_2 are the toroidal mirrors that image the input slit onto the output plane where the CCD camera is placed. M is a plane mirror, and the lens is placed at a distance f from the entrance slit.

filaments is observed). The beam has a FWHM 5-mm diameter and is then focused onto the LBO crystal with a 50-cm-focal-length lens placed 50.1 cm from the crystal entrance facet.

The angular spectra of the filament have been detected by an imaging spectrometer (Oriel Instruments, Stratford, Connecticut; 77250-M with a 1200 lines/mm grating) placed after the crystal. Figure 1 shows the experimental layout of the spectrometer. The device reconstructs without distortion the entrance slit at the output plane (the slit image is not on a curved surface, as would occur for conventional optics), with the different frequency components at different lateral positions. By placing the entrance slit in the focal plane of a focusing lens, the angular frequency distribution can be detected in a single shot. The actual spectra are captured by a CCD camera placed in the monochromator output imaging plane, the central regions require a very high dynamical range 16-bit CDD camera (Andor, Belfast, Northern Ireland; EEV 40-11) in order to avoid saturation and loss of low-power details, whereas the outer regions were characterized using a higher-spatial-resolution 8-bit camera (Pulnix, Sunnyvale, California; TM-6 CN). Note that only the angular distribution in the slit plane will be monitored, which is sufficient as long as the axial symmetry of the process is preserved. In the acquisition of the angular spectra it is very important to guarantee the possibility of single-shot acquisition. In fact although the envelope spectral shape gives the information on the small-scale structure formed in the near field, the fine interference-fringe structure in the spectra will reveal the larger features in the space–time domain. For example, a single X wave, a couple, a train, and even a chaotic gas of X waves will all produce the same envelope angular spectrum, whereas the difference between the possible realizations will appear only in the modulated fine structure of the spectrum. These fine details will fluctuate slightly from shot to shot, owing to input-pulse energy, duration, and diameter fluctuations.

4. EXPERIMENTAL RESULTS

In Fig. 2 we show the filament $1/e^2$ diameter against input pulse energy. We see that as power increases the beam diameter contracts until it reaches a "stationary" value—we identify the lowest energy for which this occurs as the corresponding critical threshold energy, E_{th}. We therefore performed all of our measurements in the energy range for which stable single filamentation occurs, i.e., from 2 to 5.6 μJ. To illustrate that the phenomenum under inspection is a general feature of optical-pulse propagation and is not particularly related to the specific material, we show in Fig. 3 two angular spectra, the first obtained in water [Fig. 3(a)] with $E \sim 2E_{\mathrm{th}}$ and the second in LBO [Fig. 3(b)] with $E \sim 1E_{\mathrm{th}}$. Figure 3(b) was obtained from three separate images, each spanning a different wavelength range (420–510 nm, 510–540 nm, 540–650 nm) so as to minimize the effects of "blooming" from the central high-intensity region while still keeping sig-

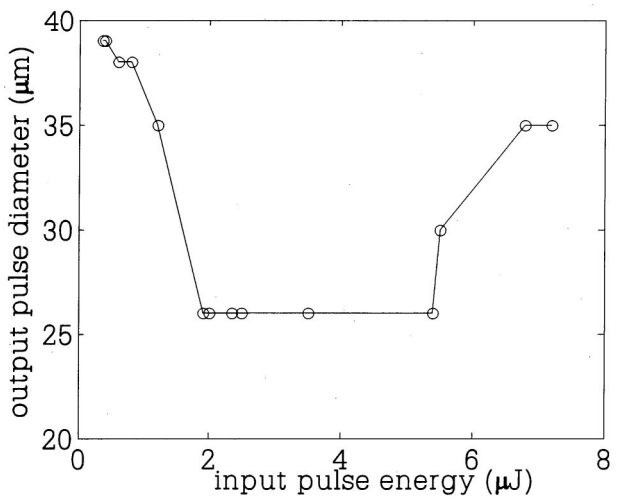

Fig. 2. Output beam diameter for varying input pulse energy. All measurements reported in this work were performed in the energy interval 2–5.6 μJ, where single filamentation was observed.

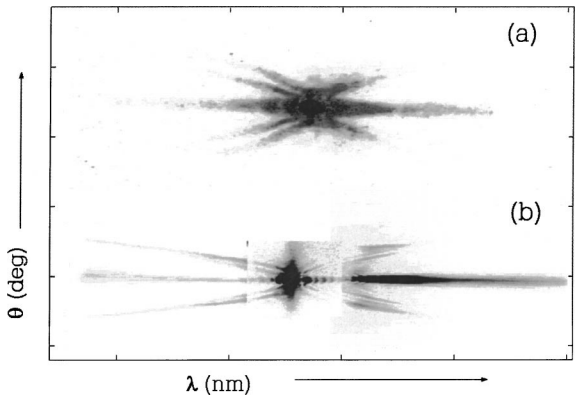

Fig. 3. Two examples of pulse-filamentation far-field spectra taken for two different materials: (a) in 15 mm of water, $P \sim 2P_{\mathrm{crit}}$ (λ ranges from 550 to 650 nm) and (b) in 15 mm of LBO, $P \sim 1P_{\mathrm{crit}}$. (b) was obtained from three separate images, each one spanning a different wavelength range (420–510 nm, 510–540 nm, 540–650 nm). θ ranges from -10 deg to $+10$ deg in each figure.

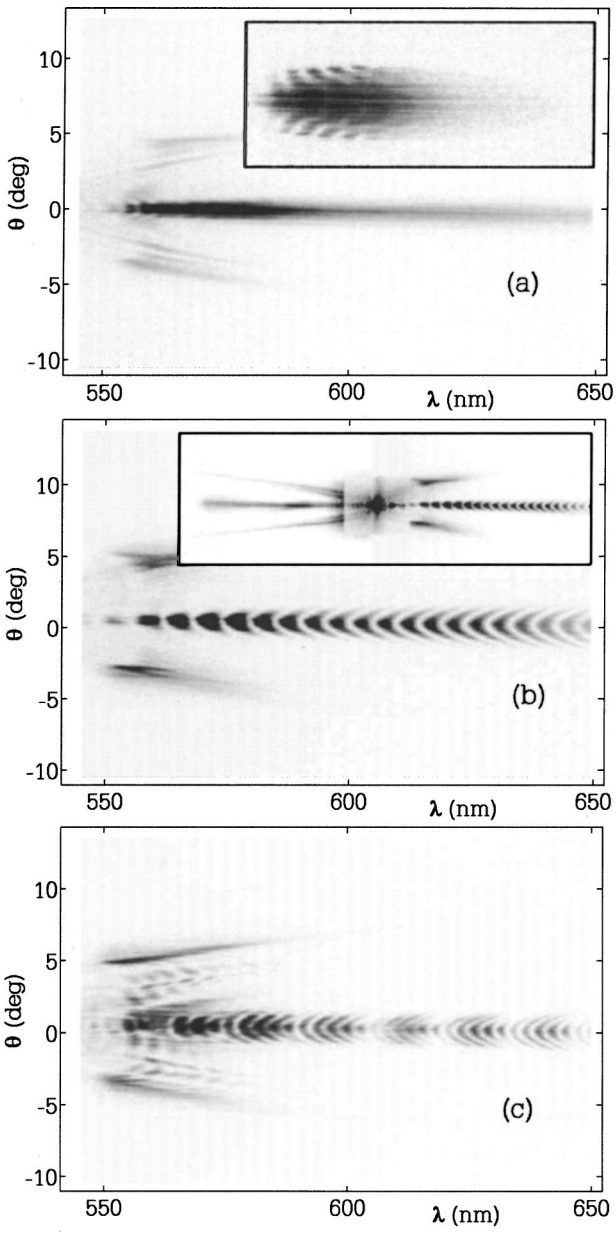

Fig. 4. Stokes component of the measured far-field spectra. (a) Input pulse energy $E_{in} = 2\ \mu J$; in the inset we show another spectrum taken for a slightly smaller E_{in} that highlights the modulation fringes. The total spectrum is shown in Fig. 3. (b) $E_{in} = 3\ \mu J$; in the inset we show the total recorded spectrum. (c) $E_{in} = 4.8\ \mu J$. Note the different modulation patterns in the three measurements.

nificant detail in the lower-intensity regions. Note that very similar spectral features have been reported elsewhere relative to filamentation of picosecond pulses in air.[30] Although Fig. 3(a) has fewer details owing the large number (30) of shots over which the profile for water was integrated, the spectra have in common a definite X-like pattern with a strong on-axis emission. We obtained similar figures for fused silica.

We shall now look more closely at the angular spectra, paying particular attention to the details. In Figs. 4(a), 4(b), and 4(c) we show the angular spectra for input energies E_{in} equal to 2, 3, and 4.8 μJ, respectively, thus mapping the evolution of the pulse structure for increasing powers. In all of these figures we have focused our attention on the Stokes part of the spectrum; the complete recorded spectrum for $E_{in} = 2\ \mu J$ is shown in Fig. 3(b) and that for $E_{in} = 3\ \mu J$ is shown in the inset of Fig. 4(b). We first note the strong on-axis (i.e., for small transverse wave vectors or angles, AE) emission that extends well both into the blue Stokes and red anti-Stokes regions, characteristic of pulse filamentation and subsequent continuum generation. If considered in frequency rather than in wavelength, the anti-Stokes components have a larger extension ($\sim 0.9\ fs^{-1}$) than the Stokes components ($\sim 0.7\ fs^{-1}$), in agreement with literature.[12,36,45] Together with the low-angle emission there is also a distinct "X" pattern, a signature of CE with a much more pronounced extension of the anti-Stokes component ($\sim 0.9\ fs^{-1}$ compared with the $\sim 0.2\ fs^{-1}$ of the Stokes part). All of the recorded spectra show a surprisingly regular pattern for small θ. This pattern is not so obvious in Fig. 4(a), so we have included in the inset the Stokes spectrum for a different laser shot in which it is much clearer. The fringes are centered at $\theta = 0$ with parabolic-like dependence on wavelength (similar features have also been observed in air with longer input pulse durations[30]). It is interesting to note how the sign of the fringe curvature inverts in when passed from $E_{in} = 2\ \mu J$ to $E_{in} = 3\ \mu J$ and then shows a further sovra-modulation for $E_{in} = 4.8\ \mu J$ (Fig. 4). We note that this behavior was also found in other materials (e.g., water) and under different focusing conditions, with the only difference being the actual input energies at which the various modulation patterns are observed.

5. DISCUSSION

Despite the large amount of data available in the literature, to the best of our knowledge none of the numerical simulations shown to date display a combination of the main features we have measured. Namely, these are the distinct X arms, the strong and largely extended axial emission, the periodic modulation of the axial emission, and, finally, the inversion of this modulation pattern with increasing input power. Given this large difference, we try to give an explanation of the spectra by studying the properties of a linear superposition of stationary states, with which we approximate the instantaneous wave forms (into which the actual pulse shape may be decomposed) inside the material. The nature of the linear states will depend on the nature of the associated spectral shape, so that CE will be related to an X-like wave[14] whereas AE may be simply related to a Gaussian-like spatiotemporal profile. We underline that the following discussion is not aimed at explaining beam filamentation but rather at trying to justify the experimental spectral features starting from results presented in literature.

We start by analyzing the spectrum for $E_{in} = 2\ \mu J$. The input power is just above P_{crit}, so that during propagation the pulse starts to collapse; in doing so a strong CE is initiated, and finally the energy is moved to the trailing edge of the filament, as discussed above. Therefore we may describe the overall pulse as an X wave (associated with the CE) and a trailing Gaussian profile. The X

wave is described following the recipe given elsewhere[32] with the input parameters taken as the material refractive index and dispersion relations and the total bandwidth of the actual measured CE (110 nm). The Gaussian profile is chosen so that it has a $1/e^2$ width equal to that measured (26 μm) and a temporal bandwidth corresponding to the measured AE bandwidth (230 nm). We note that all of the results described below do not actually depend on the particular function chosen to describe the Gaussian-like profile, and no substantial variations were observed using a super-Gaussian or hyperbolic-secant profile with respect to a simple Gaussian form. Furthermore, we may expect a temporal delay between the two profiles, and indeed it is the interference between these two that gives rise to the measured modulation patterns. However, we are still missing an ingredient. If we take the above-described pulses and Fourier transform the sum of these to obtain the angular spectra, we observe only straight, vertically aligned interference fringes. To explain the curvature of these we must also introduce a transverse spatial chirp (i.e., a phase-front curvature) into the Gaussian profile. It is well known that, in the presence of GVD and/or SPM, the pulse may develop a strong temporal chirp. It has also been noted that in the simultaneous presence of SPM and SF, the pulse may also develop a strong frequency-dependent mode size[46] and a spatial chirp. In analogy with a linear temporal chirp[47] we may write the complex spatial amplitude as $A(r) = \exp[-(1 + j\alpha_r)(r/\sigma)^2]$, where σ is the beam width and α_r is the spatial chirp parameter. Figure 5(a) shows the (θ–λ) distribution for an X wave and a spatially chirped Gaussian pulse with $\alpha_r = -2$ and temporally delayed by $\tau = -200$ fs, thus approximating the power buildup at the trailing edge of the pulse expected for low-input powers. The absolute value of α_r was chosen to match the angular divergence of the AE and the sign was chosen to match the measured fringe curvature direction. Indeed, as can be seen the axial component shows a definite curved fringe pattern in close agreement with that shown in Fig. 4(a). A negative spatial chirp (i.e., a defocusing phase-front curvature) could be due to a delayed-plasma induced defocusing. However, we note that there is another possibility, that the spatial chirp has an opposite sign ($\alpha_r = +2$) and the Gaussian pulse (shock wave) is in front of the X wave. Although a leading shock front with a focusing wave front is in fact compatible with a strong SF regime, we believe the picture of a trailing shock wave (at input powers near threshold) to be more acceptable in the frame of the present literature. Indeed, this is precisely the situation depicted in numerical studies conducted near the threshold for beam collapse ($P < 2P_{crit}$)[12,38]; during the collapse the beam evolves by pushing the energy toward the trailing edge. Subsequently, a steep shock front forms at the postion of this energy pileup, i.e., at the rear of the pulse where we therefore choose to position our linear Gaussian state.

Regarding the presence of a strong axial emission, the scientific community is still lacking a widely accepted theory, although the most-frequent explanations involve the formation of an effective waveguide[44] induced by the balance of plasma defocusing and SF or just from the effect of SF alone.[36] However, SF is just the spatial mani

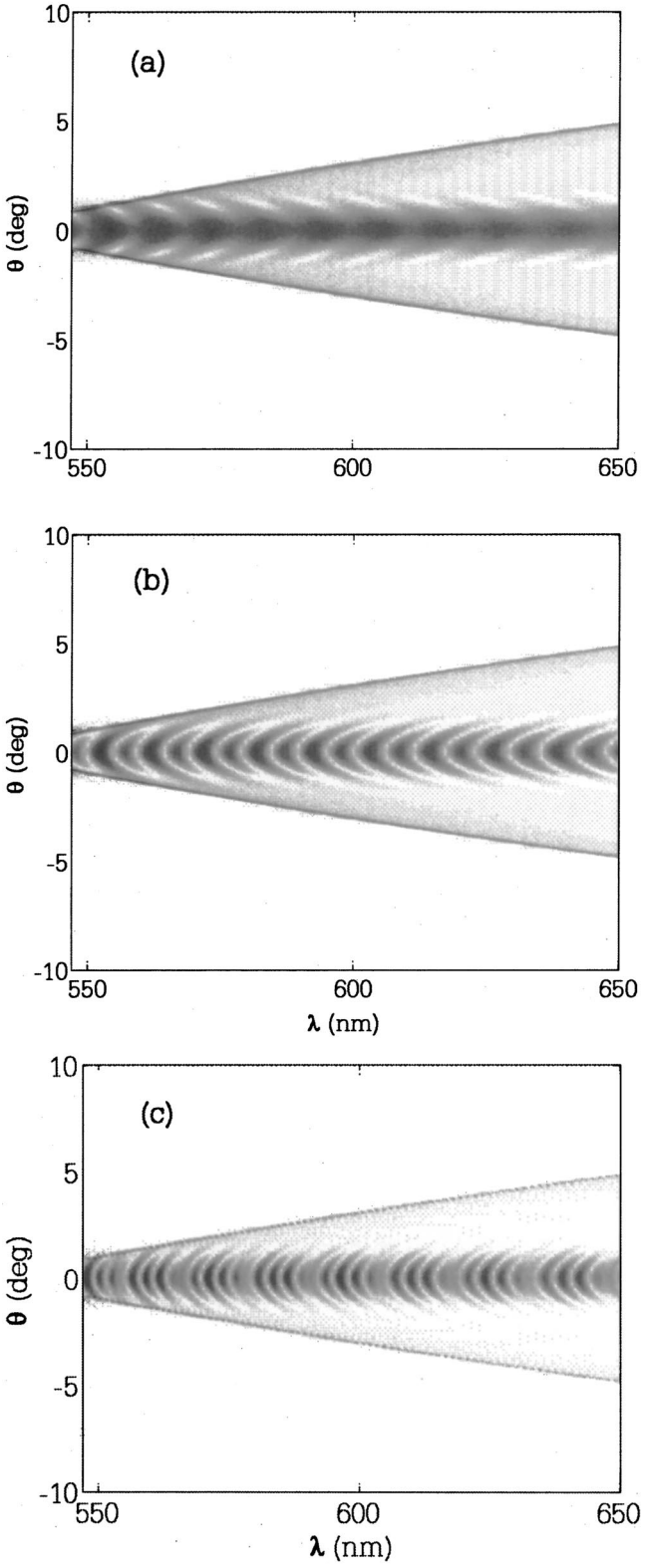

Fig. 5. Calculated far-field spectra of stationary linear states. (a) A Gaussian pulse with spatial chirp $\alpha_s = -2$ and temporally delayed by +200 fs, with respect to an X wave, (b) two equal-intensity spatially chirped Gaussian pulses temporally shifted with respect to an X wave by −220 fs ($\alpha_s = +2$) and +220 fs ($\alpha_s = -2$) and (c) three equal-intensity spatially chirped Gaussian pulses temporally shifted by −300 ($\alpha_s = +2$), −200 ($\alpha_s = +2$), and +300 fs ($\alpha_s = -2$), with an X wave in t = 0. All Gaussian radial diameters are 25 μm at $1/e^2$.

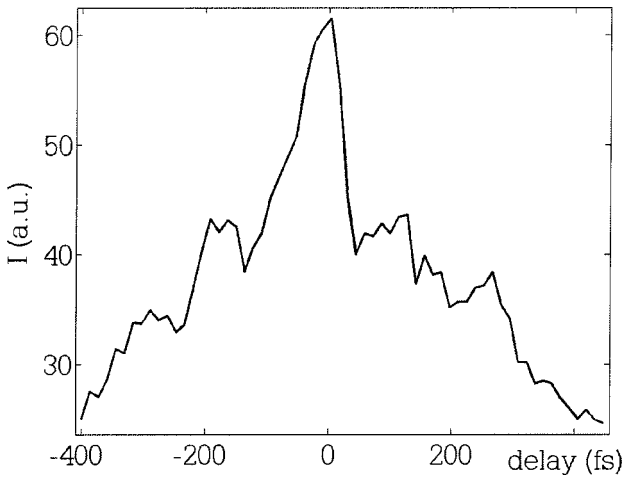

Fig. 6. Autocorrelation trace of the ouput pulse filament showing that the pulse has split into three subpulses with a delay of ~600 fs between the most external ones. $E_{\mathrm{in}} \sim 4\ \mu\mathrm{J}$.

festation of SPM. The temporal analog generates new frequencies and, in the spirit of this paper, the two should not be considered separately. Indeed, it is the spatiotemporal effect of SPM that explains CE, so it is not obvious why at a certain point of the pulse evolution SPM should split into separate spatial (SF) and temporal (spectral broadening) phenomena. We suggest that it could be possible that nonlinear losses play an important role. Numerical simulations confirm that in the presence of nonlinear losses a high-intensity pulse will develop a flat top (as also reported in literature[48]) and, correspondingly, the spectral components generated via SPM will be strongly limited. This should occur in both the spatial and the temporal coordinates. However, there may exist mechanisms that break the spatiotemporal symmetry, such as Raman nonlinearity, plasma generation, or higher-order dispersion, which in turn could force the wave collapse in the sole temporal dimension, i.e., the formation of a temporal shock wave with a spatial flat top. In this case we would observe AE, an efficient broadening of the temporal spectrum with spatial wave vectors aligned along the input pulse-propagation axis.

As for the spatial chirp, we note that the fringe pattern for higher powers is qualitatively different from that observed near P_{crit}. Indeed, not only is the curvature inverted but the modulation is also much deeper, and it is not concentrated near the central carrier frequency but rather becomes clearer at frequency shifts greater than those obtained by CE. If we take into account these features we realize that the interference is not due to an interplay between a Gaussian and an X profile but rather between two (or more) Gaussian-like pulses. Moreover, the chirp of the two pulses must have opposite signs and similar absolute values if such sharp and deep modulation patterns are to be explained. In Fig. 5(b) we kept $\alpha_r = -2$ for the rear pulse and put $\alpha_r = +2$ for the leading pulse. This condition gives us high contrast fringes with the same measured curvature shown in Fig. 4(b).

The temporal delays of the two Gaussian pulses in Fig. 5(b) where chosen to match the experimental fringe frequency, so that $\tau = -220$ and $\tau = 220$ fs with respect to a central X wave. As already discussed, we are to expect pulse splitting or dynamic replenishment for these higher-input energies. The actual position of the X component does not induce any relevant changes in the AE, and we are not able to precisely determine the temporal location of the CE. We may explain this by noting that the total power contained in the experimental spectrum related to the CE part (after the monocromator input slit) is always at least a factor of ten smaller than that due to AE, so interference between the two contributions is rather weak [see, for example, the very low contrast interference fringes in Figs. 4(a) and 5(a)]. The total delay between the leading and trailing pulses (440 fs) is surprisingly high if compared with the 200-fs input pulse duration. Obviously, dispersion (GVM between the daughter pulses) is playing a major role and is indeed dominating the temporal profile evolution.

Figure 5(c) was obtained with three such Gaussian pulses with temporal delays $\tau = -400$, -240, $+400$ and $\alpha = +2$, $+2$, and -2, respectively. Once again we were not able to precisely position the X wave as negligible variations were observed. The agreement with the experimental data [Fig. 4(c)] is very good, and the model is in agreement with other reported findings relative to the formation of multiple peak re-formation for high enough input energies.[40,49] Furthermore, the temporal delay between the pulses has increased to 800 fs, i.e., four times the input-pulse duration, and indicates that for higher powers the interplay between SPM, SC generation, and GVD is further enhanced, as expected. This delay is extremely large if compared with the input-pulse duration; however, a further indication that this result is correct is given by the multiple-shot autocorrelation trace shown in Fig. 6 obtained by imaging the output crystal facet onto the autocorrelation nonlinear crystal. Although the autocorrelation trace is rather noisy, we see five peaks that show that, with a similar average pulse input energy, we have multiple pulse splitting with the formation of three daughter pulses and a temporal separation of ~600 fs between the leading and trailing pulses.

So far, we have purposely neglected temporal chirp (α_t), which is expected to be at least as important as the spatial chirp. However, AE does not seem to be sensitive to this parameter. Indeed, variations of α_t did not produce a significant change in the numerical AE fringe pattern but rather only a local reduction of contrast, the position of which depends on the sign and value of α_t in the various linear components with which the filament was modeled. We note, however, that the experimental spectra also show a modulation in the CE in the form of a multiple X-arm splitting. This sheds some light on the nature of the CE in the sense that it may be explained by superimposing multiple X pulses so that the number of arms corresponds directly to the number of X pulses and each X must be spectrally shifted with respect to the others. This is physically feasible in the presence of a single input pulse that undergoes severe temporal chirping and then splits into multiple X pulses (i.e., daughter pulses that give rise to CE) so that each of these is centered on a different carrier frequency. The values for the spectral shift observed in our spectra vary from 0.05 to 0.2 fs^{-1}, with the higher values observed at higher input energies.

6. CONCLUSIONS

In conclusion we have shown the possibility of recovering detailed information regarding space–time coupled phenomena from angular-spectral characterization. The nature of the numerical model used to interpret the experimental measurements, based on a linear combination of stationary states rather than on a full nonlinear evolution simulation, allows only a qualitative guess at the parameters involved. Nevertheless, the simplicity of this approach is very appealing, and indeed by use of a combination of linear states it is possible to understand if the pulse has changed its spatiotemporal energy distribution without actually experiencing splitting or if it has gone through a single (or even multiple) pulse reformation. The details of the spectra also reveal that the spatiotemporal coupling manifests itself in a strong spatial chirp of the filament. If the far-field measurements were to be completed with a complete phase characterization, we would of course be able to reconstruct the full space–time profile of the pulse through a Fourier transform; the lack of this information is reflected in the difficulty in retrieving more precise information, for example, of the exact temporal delay of the CE with respect to the AE sources. Furthermore, the spatial chirp parameter may be determined precisely with the combination of an imaging spectrometer and a spatial shearing interferometer[50] and shall be considered in future measurements. We further underline that whereas the X part of the spectra are numerically well reproduced in the frame of our simple linear model in both the Stokes and anti-Stokes regions, this is not true for the AE spectral components. The anti-Stokes AE is rather confused and the (not always visible) fringe pattern seems to show a fast modulation frequency that is not compatible with the parameters that fit the Stokes region. This could indicate that the shock waves that generate the blueshifts and redshifts in the spectrum are spatially distinct and have different temporal delays.

Notwithstanding these shortcomings, the aim of this work is to underline the importance of angular spectral measurements that, together with other methods such as FROG or three-dimensional mapping, may give a complete and exhaustive characterization of nonlinear optical-wave collapse phenomena.

*D. Faccio's e-mail address is daniele.faccio@uninsubria.it.

†Present address, Institut de Ciències Fotòniques, c/Jordi Girona 29, NEXUS II, E-08034 Barcelona, Spain.

‡Present address, Laboratoire Kastler Brossel, Université Pieme et M. Curie, Case74, 4, place Jussieu, F75252 Paris, France

REFERENCES

1. R. Y. Chiao, E. Garmire, and C. H. Townes, "Self focusing optical beams," Phys. Rev. Lett. **13**, 479–482 (1964).
2. P. L. Kelley, "Self-trapping of optical beams," Phys. Rev. Lett. **15**, 1005–1008 (1965).
3. M. Hercher, "Laser-induced damage in transparent media," J. Opt. Soc. Am. **54**, 563 (1964).
4. P. Lallemand and N. Bloembergen, "Self-focusing of laser beams and stimulated Raman gain in liquids," Phys. Rev. Lett. **15**, 1010–1012 (1965).
5. A. Braun, G. Korn, X. Liu, D. Du, J. Squier, and G. Mourou, "Self-channeling of high-peak-power femtosecond laser pulses in air," Opt. Lett. **20**, 73–75 (1995).
6. K. Wilson and V. Yakovlev, "Ultrafast rainbow: tunable ultrashort pulses from a solid-state kilohertz system," J. Opt. Soc. Am. B **14**, 444–448 (1997).
7. R. Alfano, *The Supercontinuum Laser Source* (Springer-Verlag, New York, 1989).
8. P. Rairoux, H. Schillinger, S. Niedermeier, M. Rodriguez, F. Ronneberger, R. Sauerbrey, B. Stein, D. Waite, C. Wedekind, H. Wille, L. Wöste, and C. Ziener, "Remote sensing of the atmosphere using ultrashort laser pulses," Appl. Phys. B: Photophys. Laser Chem. **71**, 573–580 (2000).
9. P. Nozieres and D. Pines, *The Theory of Quantum Liquids, Vol. II* (Addison-Wesley, Redwood City, 1990).
10. D. Strickland and P. Corkum, "Resistance of short pulses to self-focusing," J. Opt. Soc. Am. B **11**, 492–497 (1994).
11. G. Luther, A. Newell, J. Moloney, and E. Wright, "Short pulse conical emission and spectral broadening in normally dispersive media," Opt. Lett. **19**, 789–791 (1994).
12. A. Gaeta, "Catastrophic collapse of ultrashort pulses," Phys. Rev. Lett. **84**, 3582–3585 (2000).
13. J. Ranka and A. Gaeta, "Breakdown of the slowly varying envelope approximation in the self-focusing of ultra-short pulses," Opt. Lett. **23**, 534–536 (1998).
14. S. Trillo, C. Conti, P. D. Trapani, O. Jedrkiewicz, J. Trull, G. Valiulis, and G. Bellanca, "Coloured conical emission via second-harmonic generation," Opt. Lett. **27**, 1451–1453 (2002).
15. G. Valiulis, J. Kilius, O. Jedrkiewicz, A. Bramati, S. Minardi, C. Conti, S. Trillo, A. Piskarskas, and P. Di Trapani, "Space-time nonlinear compression and three-dimensional complex trapping in normal dispersion," in *Quantum Electronics and Laser Science Conference*, Vol. 57 of OSA Trends in Optics and Photonics Series (Optical Society of America, Washington D.C., 2001), postconference edition, pp. QPD10-1-2.
16. P. Di Trapani, G. Valiulis, A. Piskarskas, O. Jedrkiewicz, J. Trull, C. Conti, and S. Trillo, "Spontaneously generated X-shaped light bullets," Phys. Rev. Lett. **91**, 093904 (2003).
17. C. Conti, S. Trillo, P. Di Trapani, G. Valiulis, A. Piskarskas, O. Jedrkiewicz, and J. Trull, "Nonlinear electromagnetic X waves," Phys. Rev. Lett. **90**, 170406 (2003).
18. O. Jedrkiewicz, J. Trull, G. Valiulis, A. Piskarskas, C. Conti, S. Trillo, and P. Di Trapani, "Nonlinear X wavesin second harmonic generation: experimental results," Phys. Rev. E **68**, 026610 (2003).
19. D. Salerno, O. Jedrkiewicz, P. Di Trapani, J. Trull, and G. Valiulis, "Impact of dimensionality on noise-seeded modulational instability," in *Nonlinear Guided Waves and their Applications* (Optical Society of America, Washington, D.C., 2004), pp. WA-7.
20. S. Minardi, J. Yu, G. Blasi, A. Varanavičius, G. Valiulis, A. Beržanskis, A. Piskarskas, and P. Di Trapani, "Red solitons: evidence of spatiotemporal instability in $\chi^{(2)}$ spatial soliton dynamics," Phys. Rev. Lett. **91**, 12390 (2003).
21. M. Kolesik, E. Wright, and J. Moloney, "Dynamic nonlinear X-waves for femtosecond pulse propagation in water," Phys. Rev. Lett. **92**, 253901 (2004).
22. A. Dubietis, E. Gaizauskas, G. Tamosauskas, and P. Di Trapani, "Light filaments without self-channeling," Phys. Rev. Lett. **92**, 253903 (2004).
23. S. Diddams, H. Eaton, A. Zozulya, and T. Clement, "Amplitude and phase measurements of femtosecond pulse splitting in nonlinear dispersive media," Opt. Lett. **23**, 379–381 (1998).
24. A. Bernstein, J. Diels, T. Luk, T. Nelson, A. McPherson, and S. Cameron, "Time resolved measurements of self focusing pulses in air," Opt. Lett. **28**, 2354–2356 (2003).
25. L. Gallmann, G. Steinmeyer, D. Sutter, T. Rupp, C. Iaconis, I. Walmsley, and U. Keller, "Spatially resolved amplitude and phase characterization of femtosecond optical pulses," Opt. Lett. **26**, 96–98 (2001).
26. C. Dorrer, E. Kosik, and I. Walmsley, "Direct space-time

characterization of the electric fields of ultrashort optical pulses," Opt. Lett. **27**, 548–550 (2002).
27. M. Potenza, S. Minardi, J. Trull, G. Blasi, D. Salerno, A. Varanavičius, A. Piskarskas, and P. Di Trapani, "Three dimensional imaging of short pulses," Opt. Commun. **229**, 381–390 (2004).
28. J. Trull, O. Jedrkiewicz, P. Di Trapani, A. Matijosius, A. Varanavičius, G. Valiulis, R. Danielius, E. Kucinskas, and A. Piskarskas, "Spatiotemporal three-dimensional mapping of nonlinear X-waves," Phys. Rev. E **69**, 026607 (2004).
29. A. Matijosius, J. Trull, P. Di Trapani, A. Dubietis, R. Piskarskas, A. Varanavičius, and A. Piskarskas, "Nonlinear space-time dynamics of ultrashort wave packets in water," Opt. Lett. **29**, 1123–1125 (2004).
30. D. Mikalauskas, A. Dubietis, and R. Danielius, "Observation of light filaments induced in air by visible picosecond laser pulses," Appl. Phys. B: Photophys. Laser Chem. **75**, 899–902 (2002).
31. A. Dubietis, G. Tamošauskas, I. Diomin, and A. Varanavičius, "Self-guided propagation of femtosecond light pulses in water," Opt. Lett. **28**, 1269–1271 (2003).
32. M. Porras and P. Di Trapani, "Localized and stationary light wave modes in dispersive media," Phys. Rev. E **69**, 066606-1 (2004).
33. J. Marburger, "Self-focusing: theory," Prog. Quantum Electron. **4**, 35–110 (1975).
34. P. Chernev and V. Petrov, "Self-focusing of light pulses in the presence of normal group-velocity dispersion," Opt. Lett. **17**, 172–174 (1992).
35. G. Luther, J. Moloney, A. Newell, and E. Wright, "Self-focusing threshold in normally dispersive media," Opt. Lett. **19**, 862–864 (1994).
36. A. Brodeur and S. Chin, "Ultrafast white light continuum generation and self-focusing in transarent condensed media," J. Opt. Soc. Am. B **16**, 637–650 (1999).
37. A. Zozulya and S. A. Diddams, "Dynamics of self-focused femtosecond laser pulses in the near and far fields," Opt. Express **4**, 336–343 (1999), http://www.opticsexpress.org.
38. J. Rothenberg, "Space-time focusing: breakdown of the slowly varying envelope approximation in the self-focusing of femtosecond pulses," Opt. Lett. **17**, 1340–1342 (1992).
39. M. Mlejnek, E. Wright, and J. Moloney, "Dynamic spatial replenishment of femtosecond pulses propagating in air," Opt. Lett. **23**, 382–384 (1998).
40. M. Mlejnek, E. Wright, and J. Moloney, "Power dependence of dynamic spatial replenishment of femtosecond pulses propagating in air," Opt. Express **4**, 223–228 (1999), http://www.opticsexpress.org.
41. O. Kosareva, V. Kandidov, A. Brodeur, C. Chen, and S. Chin, "Conical emission from laser-plasma interactions in the filamentation of powerful ultrashort laser pulses in air," Opt. Lett. **22**, 1332–1334 (1997).
42. S. Tzortzakis, L. Sudrie, M. Franco, B. Prade, A. Mysyrowicz, A. Couairon, and L. Bergé, "Self-guided propagation of ultrashort IR laser pulses in fused silica," Phys. Rev. Lett. **87**, 213902 (2001).
43. W. Smith, P. Liu, and N. Bloembergen, "Superbroadening in H_2O and D_2O by self focused picosecond pulses from a YAlG:Nd laser," Phys. Rev. A **15**, 2396–2403 (1977).
44. E. Nibbering, P. Curley, G. Grillon, B. Prade, M. Franco, F. Salin, and A. Mysyrowicz, "Conical emission from self guided femtosecond pulses in air," Opt. Lett. **21**, 62–64 (1996).
45. W. Liu, O. Kosareva, I. Golubtsov, A. Iwasaki, A. Becker, V. Kandidov, and S. Chin, "Femtosecond laser pulse filamentation versus optical breakdown in H_2O," Appl. Phys. B: Photophys. Laser Chem. **76**, 215–229 (2003).
46. S. Cundiff, W. Knox, E. Ippen, and H. Haus, "Frequency dependent mode size in broadband Kerr-lens mode locking," Opt. Lett. **21**, 662–664 (1996).
47. S. Polyakov, F. Yoshino, and G. Stegeman, "Interplay between self-focusing and high-order multiphoton absorption," J. Opt. Soc. Am. B **18**, 1891–1895 (2001).
48. S. Akhmanov, V. Vysloukh, and A. Chirkin, *Optics of Femtosecond Laser Pulses* (American Institute of Physics, New York, 1992).
49. W. Liu, S. Chin, O. Kosareva, I. S. Golubtsov, and V. Kandidov, "Multiple refocusing of a femtosecond laser pulse in a dispersive liquid (methanol)," Opt. Commun. **225**, 193–209 (2003).
50. C. Dorrer and I. Walmsley, "Simple linear tecnique for the measurement of space-time coupling in ultrashort optical pulses," Opt. Lett. **27**, 1947–1949 (2002).